ChemBioChem

Research Article
doi.org/10.1002/cbic.202400930

Chemistry Europe
European Chemical Societies Publishing

www.chembiochem.org

Proton Occupancies in Histidine Side Chains of Carbonic Anhydrase II by Neutron Crystallography and NMR – Differences, Similarities and Opportunities

Suzanne Zoë Fisher,[a, b] Heiner N. Raum,[c, d] and Ulrich Weininger*[c]

Histidine is a key amino-acid residues in proteins that can exist in three different protonation states: two different neutral tautomeric forms and a protonated, positively charged one. It can act as both donor and acceptor of hydrogen bonds, coordinate metal ions, and engage in acid/base catalysis. Human Carbonic Anhydrase II (HCA II) is a pivotal enzyme catalyzing the reversible hydration of carbon dioxide. It contains 12 histidine residues: six are surface exposed, two buried, three are active site zinc ion ligands, and one is a proton shuttle. Comparing results from NMR spectroscopy with previously determined neutron protein crystal structures enabled a side-by-side investigation of the proton occupancies and preferred tautomeric states of the histidine residues in HCA II. Buried and zinc coordinating histidines remain in one neutral tautomeric state across the entire pH range studied, as validated by both methods. In contrast, solvent-exposed histidines display high variability in proton occupancies. While the data were overall remarkably consistent between methods, some discrepancies were observed, shedding light on the limitations of each technique. Therefore, combining these methods with full awareness of the advantages and drawbacks of each, provides insights into the dynamic protonation landscape of HCA II histidines, crucial for elucidating enzyme catalytic mechanisms.

Introduction

Hydrogens bound to nitrogen and oxygen are polarized and exchangeable. This makes them especially important for the structure, stability, and function of proteins and enzymes in particular. These hydrogens are involved in hydrogen bonds,[1] while the presence or absence of an additional proton alters the charge in ionizable groups and thereby affects Coulomb interactions.[2–4] Hydrogen bonds and Coulomb interactions form the basis for structure, stability, binding of ligands, and ultimately the functions of proteins. Furthermore, the transfer of protons is a key enzymatic process involved in many types of enzyme-catalyzed reactions.[5,6] Due to the fundamental role of hydrogen in biology, there is a need to know where and to what extent these protons are located in the structure of a protein. While this is easily known for backbone amide groups, it cannot reliably be predicted or easily experimentally observed for ionizable side chains, such as aspartate, glutamate, histidine, cysteine, tyrosine, lysine, and arginine, as well as in ordered water, catalytically activated water (e.g., H_3O^+ or OH^-), ligands, or cofactors.

Histidine is chemically the most versatile amino acid, and therefore commonly involved mediating enzyme catalysis, such as general acid/base chemistry.[7,8] It can exist in three different states, depending on the location of the imidazole protons: one protonated and positively charged (His^+), with protons on both Nε2 and Nδ1, and two neutral (HNε2 and HNδ1) tautomeric forms[9], with one proton on either Nε2 or Nδ1 (Figure 1). It often exists in two or three states simultaneously at equilibrium,[10] and these can interconvert rapidly.[11] Due to this versatile nature of histidine, it can have a variety of functions, including coordinating metal ions,[12] as a nucleophile, an acid/base catalyst,[5,6] a proton shuttle[13,14] or as a hydrogen bond donor and acceptor.[15,16] The potential of acting both as a hydrogen donor and acceptor make histidines a crucial part in hydrogen bond networks, as exemplified in photosystem II,[17,18] Pin1,[19] and regulating ion channels.[20,21]

Neutron crystallography of proteins,[22,23] and in rare instances ultra-high-resolution x-ray crystallography, provides an atomic resolution view of the explicit positions of hydrogen atoms. This is due to the strong scattering interactions of neutrons with hydrogen atomic nuclei and enables the discrimination between isotopes of hydrogen, specifically ^1H (protium, or H) and ^2H (deuterium, or D). With selective

[a] S. Zoë Fisher
Department of Biology & Lund Protein Production Platform, Lund University, Sölvegatan 35, SE_22362 Lund, Sweden

[b] S. Zoë Fisher
Scientific Activities Division, European Spallation Source ERIC, P.O. Box 176, SE-22100 Lund, Sweden

[c] H. N. Raum, U. Weininger
Institute of Physics, Biophysics, Martin-Luther-University Halle-Wittenberg, D-06120 Halle (Saale), Germany
Phone: +49 345 55 28555
Fax: +49 345 55 27161
E-mail: ulrich.weininger@physik.uni-halle.de

[d] H. N. Raum
Clinic for Radiology, University of Münster and University Hospital Münster, D-48149 Münster, Germany

Supporting information for this article is available on the WWW under https://doi.org/10.1002/cbic.202400930

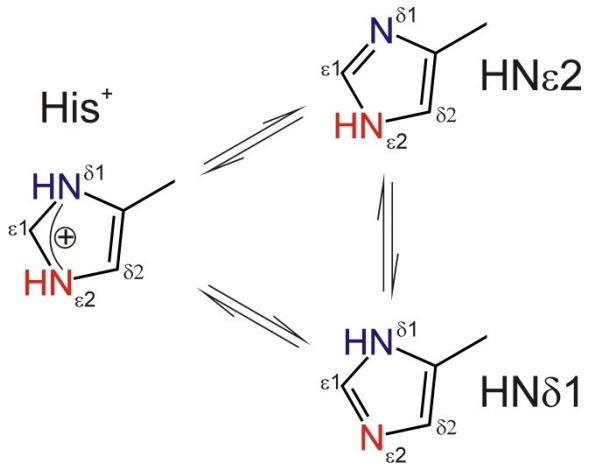

Figure 1. Protonation states of histidine at equilibrium. Positions within the imidazole ring are labeled. ε2 positions are colored red, δ1 position are colored blue.

deuteration (substitution of ^{1}H with ^{2}H) it is possible to benefit from the strong positive scattering from ^{2}H and determine hydrogen atom positions at even modest ~2.5 Å resolution.[24] However, neutron scattering from ^{1}H is negative and if deuterium-labeling (deuteration) is incomplete and either isotope is present the negative scattering from residual ^{1}H lead to signal cancellation. The net result is that neutron scattering length density maps for partially deuterated or H/D exchanged protein can be very challenging to analyze.[25] For deuterated proteins, the method can be used to identify the protonation/charged state of amino acid side chains, directly visualize hydrogen bonds, and also to distinguish between different water species (e.g. D_2O can be distinguished from D_3O^+).[26] It should be pointed out that neutron protein crystal structures can be difficult to study as there are inherent challenges such as diffraction data completeness, resolution, and signal-to-noise and great care has to be taken when refining and analyzing the resulting models. Despite these challenges, neutron protein crystallography is the only method that enables the direct determination of hydrogen atom positions at medium resolution (1.8 – 2.5 Å). In contrast, NMR spectroscopy is extremely powerful in determining exact proton occupancies of individual side chains of the solution ensemble in a pH dependent manner[10,27–29] and can be used to distinguish between the neutral tautomeric states.[30,31] Furthermore, NMR can determine the kinetic parameters of proton exchange as has been shown for Asp, Glu[32] and His.[11]

Human Carbonic Anhydrase II (HCA II) is a highly efficient enzyme that catalyzes the reversible conversion of carbon dioxide and water to form bicarbonate and a proton.[13,33] The catalytic step is performed by a zinc-bound hydroxide or water, while the rate limiting step is the proton transfer between the active site and the buffer or bulk solvent. The proton transfer steps are mediated by a hydrogen-bonded network of water molecules to the proton shuttling residue His64.[34–37] HCA II contains 12 histidine residues in total (Figure 2). The proton

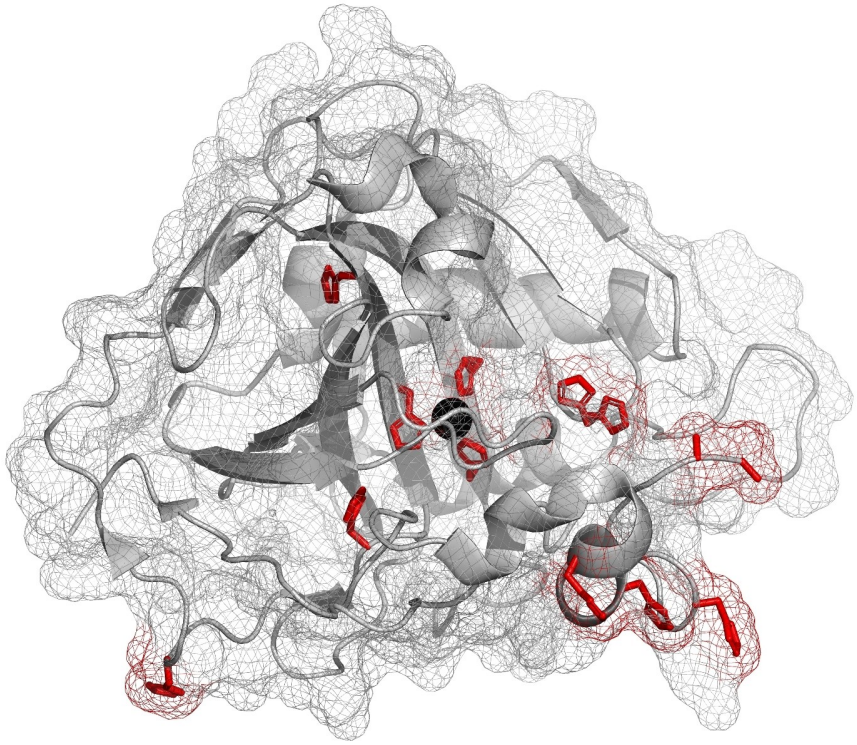

Figure 2. Ribbon diagram of HCA II with all His residues shown in red ball-and-stick representation to indicate their relative location. The zinc ion located in the active site is shown as a black sphere.

shuttle His64, three histidines coordinating the active site zinc ion (His94, His96, His119), two residues buried in the core (His107 and His122) and six solvent exposed histidines located on or close to the surface (His3, His4, His10, His15, His17 and His36). Due to the central role that His64 plays in HCA II catalysis, its proton shuttling abilities have been studied extensively by X-ray and neutron crystallography, NMR and computational methods.[14,36–42]

In this study we expand our view to include all histidine residues in HCA II and performed a detailed investigation to compare experimentally determined proton occupancies on the Nε2 and Nδ1 position in the imidazole moiety of histidine residues. We compare histidine proton occupancies determined using NMR spectroscopy in this work with similar information derived from previously determined neutron crystal structures. We highlight where both methods provide similar results, and discuss cases where they differ and offer reasons for any discrepancies. In general, neutron crystallography is the method of choice for static, averaged, one state, interior histidines, because it provides structural context and hydrogen bond networks, besides the proton occupancies of these histidines. In contrast, NMR spectroscopy is advantageous for dynamic, multiple state histidines at the surface. However, for many cases there is limited certainty in the proton occupancy of histidines by one method, which can be improved by using both methods, which is well suited for medium sized proteins like HCA II.

Results and Discussion

Histidine Location and Distribution in HCA II

Carbonic Anhydrase II contains 12 histidines, six are surface exposed and six located in the inside (Figure 2). From the six surfaced exposed histidines, five are located in the N-terminal region (His3, His4, His10, His15 and His17), the sixth one (His36) is more distantly located from all other His. The proton shuttle His64 sits on the edge of the active site and is highly dynamic and solvent exposed. The remaining five histidines in the interior consist of the three zinc ligands (His94, His96 and His119) and His107 and His122. The latter two are buried in the hydrophobic core of HCA II. Histidine signals in the NMR spectra have been assigned and some determined pK_a values have been reported by us and others previously.[14,42]

In this work we report the pK_a values as well as the derived populations of the two neutral tautomeres (HNε2 and HNδ1) for all 12 assigned Histidine residues (Table 1 and 2), with the exception of His64, which shows a very complex behaviour investigated in detail elsewhere.[14] From this information, one can calculate the population of all three states (His^+, HNε2 and HNδ1) at any given pH value. These values arise from the combination of the three different states of histidine: His^+, HNε2 and HNδ1, and their corresponding nitrogen-bound protons. Specifically, His^+ has two protons on both Nε2 and Nδ1, HNε2 with one proton on Nε2, and HNδ1 with one proton on Nδ1. We explicitly do this for pH 6 and 10, in order to compare them with neutron crystal structures determined at the same pH values. Please note that NMR results obtained at 37 °C are consistent with results from neutron crystallography at room temperature, as the pK_a values and chemical shift differences (Δδ) are unaffected by the different experimental temperatures.[14]

Table 1. NMR derived experimental pK_a values, Hill coefficient and % of the HNε2 tautomer (compared to the HNδ1 tautomer) in the neutral form.

His #	pK_a	Hill	$p_{HNε2}/p_{HNε2}+p_{HNδ1}$/%
3	6.1 ± 0.1	0.62 ± 0.04	71–85
4	6.2 ± 0.1	0.74 ± 0.04	60–72
10	5.6 ± 0.1	0.79 ± 0.07	79–93
15	5.6 ± 0.1	0.92 ± 0.07	76–90
17	5.6 ± 0.1	–	30–70[a]
36	6.94 ± 0.02	–	57–69
64 "in"	6.25 ± 0.08	–	44–56
64 "out"	7.60 ± 0.06	–	44–56
94	< 3.5		0
96	< 3.5		0
107	< 3.5		0
119	< 3.5		100
122	< 3.5		0

[a] no ^{13}Cδ signal observable, because of exchange broadening of two equally populated neutral tautomeres

Table 2. Proton occupancies (in %) determined by NMR at pH 6 and 10. The conclusion of the main tautomeric state is displayed in bold, if both are bold the histidine is mainly charged. For His^+, both positions are occupied.

	pH 6		pH 10	
His #	HNδ1	HNε2	HNδ1	HNε2
3	58–70	86–94	15–29	71–85
4	67–78	82–90	28–40	60–72
10	32–51	85–96	7–21	79–93
15	32–51	82–94	10–24	76–90
17	47–80	47–80	30–70	30–70
36	93–94	95–97	31–43	57–69
94[a]	100	0	100	0
96[a]	100	0	100	0
107[a]	100	0	100	0
119[a]	0	100	0	100
122[a]	100	0	100	0

[a] derived from the ^{2}J ^{1}H-^{15}N HSQC

Buried Histidine Residues Remain Neutral and Exist in One Tautomeric State

While NMR pH titrations allow the exact determination of the percentage of protonated, charged states versus the neutral

states at any pH value, the estimation of the HNε2 and HNδ1 distribution is often only based on reference chemical shifts and therefore has an inherent higher uncertainty. Additional ^{2}J $^{1}H^{15}N$ experiments, which are possible for static, single state histidines

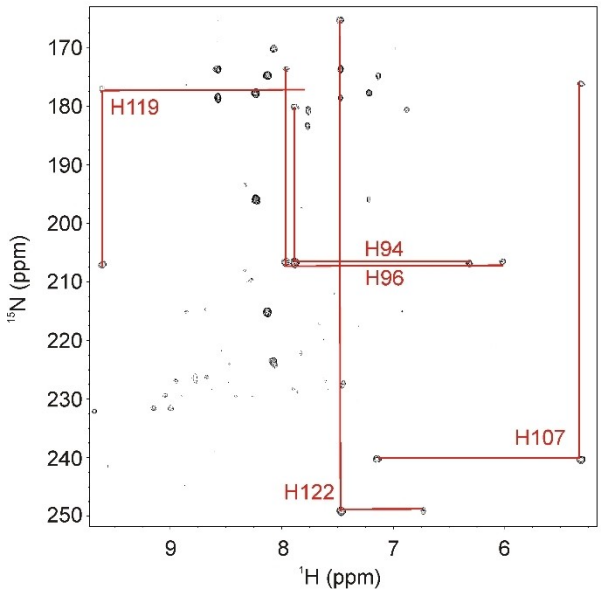

Figure 3. Histidine ^{2}J ^{1}H-^{15}N HSQC spectrum of Carbonic Anhydrase II. The patterns of cross signals for the five histidines in the interior are shown in red. They show that H107 and H122 exist 100% in the HNδ1 state. Furthermore, they show, that for H94 and H96 HNδ1 is the dominant neutral state, while for H119 it is HNε2. Together with no changes in the pH titration profiles (no population of His^{+}) one can conclude they exist in HNδ1 (H94 and H96) and HNε2 (H119) 100%.

Table 3. Refined occupancy and B-factor for ^{2}HNδ1 and ^{2}HNε2 derived from joint X-ray and neutron refined crystal structures determined at pH 6. Corresponding figures can be seen in Figure S1. The conclusion of the main tautomeric state is displayed in bold, if both are bold the histidine is mainly charged.

	pH 6		pH 10	
His #	^{2}HNδ1 occupancy (B-factor)	^{2}HNε2 occupancy (B-factor)	HNδ1 occupancy (B-factor)	HNε2 occupancy (B-factor)
3[a]	–	–	–	–
4[a]	–	–	–	–
10	0.0 (74)[b]	0.0 (84)[b]	1.0 (55)	n/a
15	n/a	0.2 (51)	n/a	0.2 (31)
17	0.2 (51)[b]	0.2 (52)[b]	n/a	0.0 (30)[b]
36	0.8 (52)	0.8 (69)	n/a	1.0 (45)
94[c]	0.8 (47)	–	1.0 (14)	–
96[c]	0.4 (31)	–	0.6 (15)	–
107	0.4 (39)	n/a	0.7 (15)	n/a
119[c]	–	0.8 (44)	–	0.8 (13)
122	1.0 (45)	n/a	0.6 (15)	n/a

[a] disordered, meaning no or very poor corresponding density in electron and nuclear scattering length density maps. [b] poor or ambiguous signal in nuclear scattering length density. [c] His64, His96, and His119 are Zn-ligands.

of medium size proteins like HCA II (Figure 3), also enable direct observation of their tautomeric state (Table 2), since the chemical shift of proton-free ^{15}N (240–250 ppm) is significantly different from the proton-bound ^{15}N chemical shift in either the neutral (165–170 ppm) or protonated form (175–185 ppm).[30] However, the chemical shift of proton-free ^{15}N can be lowered to around 210 ppm upon phosphorylation[30] or metal coordination. This is in agreement with their ^{13}Cδ chemical shifts. The histidine zinc ligands were found to be in the HNδ1 (His94 and His96) and HNε2 tautomer (His119) form, and this also supported by the neutron crystal structures determined at pH 6 and 10[43]. Based on the chemical shifts alone it is not possible to rule out the presence of some tiny percentage of protonated state for His94, His96, and His119. However, this can be dismissed since their resonances are unaffected by pH changes down to pH 5. Two other His residues that do not change tautomer or protonation state over the pH range studied are His107 and His122. Both appear to be neutral and predominantly in the HNδ1 tautomer (Figure 3, Table 2), with close to perfect ^{15}N chemical shift matches.

The same preference is observed in the neutron crystal structures at pH 6 and 10 (Table 3), that have been re-analyzed using modern software and extensive manual inspections (see Experimental Section). In fact, this approach leads to significant improvements and clarity of the neutron crystal data. The neutral state of His107 is promoted by two interactions: as a hydrogen bond donor to Glu117 and an acceptor from Tyr194 (Figure 4). The crystallographic refined occupancy and associated B-factor parameters for both pH 6 and 10 are shown in Table 3, while no density is observed for ^{2}HNε2. The situation is similar for His122 with it being a hydrogen bond donor to the backbone carbonyl of Ala142 and acceptor from Tyr51 (Figure 4). In the case of buried and zinc-bound histidines (His94, His96, His107, His119 and His122) we have excellent agreement between NMR and neutron crystallography (Figure S1).

Proton Occupancies for Solvent-Exposed His at pH 6 and 10

NMR based proton occupancies (in %) of the Nε2 and Nδ1 position for all histidines in CAII for pH 6 and pH 10 are shown in Table 2, with exception of His64 which exhibits very complex behaviour investigated elsewhere.[14] Proton occupancies can also be *roughly* estimated by neutron crystallography, but the precision is low since occupancy is computationally tied to the B-factor (a refinable parameter that indicates relative disorder or positional uncertainty) and its magnitude reflects competing scattering signals from ^{1}H and ^{2}H in partial deuteration, as explained in detail above[44]. As such, these values have to be approached with caution and not over-interpreted. At best, refined occupancy and B-factors can be used to indicate a trend and should be viewed relative to the values of other atoms.[44] The occupancy and B-factor parameters for ^{2}H atoms on histidine side chains at pH 6 and 10 are summarized in Table 3.

While the data for zinc ligand histidines, His107, and His122 are consistent and very well matched between NMR and neutron crystallography, the situation is more complicated for

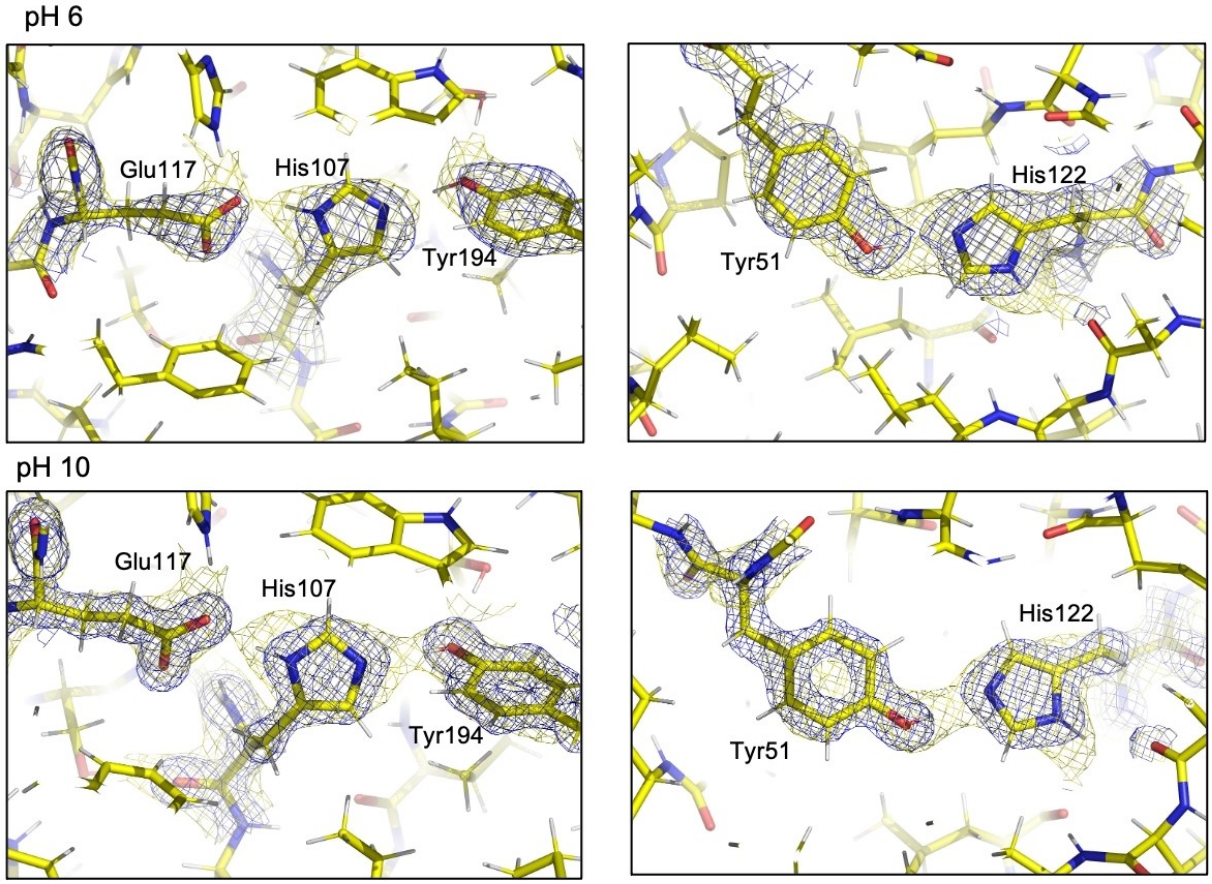

Figure 4. Buried His residues protonation states as determined by NMR and neutron protein crystallography. (a) pH 6, (b) pH 10. 2Fo–Fc nuclear scattering length and electron density maps are shown in yellow and blue, respectively, and both map types are contoured at 1.5 sigma.

the solvent exposed and dynamic histidines (His3, His4, His10, His15, His17 and His 36). These residues are vulnerable to solvent pH changes as they are on – or close to – the surface, solvent exposed, and not engaged in strong hydrogen bonds. As such, they can be expected to exist in multiple protonation states. In addition, their side chain mobility further 'smears' the signal and complicates the analysis. For these His residues, the interpretation can at best indicate or suggest a possible preferred tautomer or charged state. Great care, and even some skepticism, must to be taken when looking at the maps and refined parameters, as it is easy to extend the analysis past what the data can actually support.

While it was possible to determine preferred tautomer and proton occupancies for His3 and His4 using NMR, these N-terminal residues are completely disordered (invisible) in the crystal structures and we observe almost no density for them. His15, His17, and His36 follow broadly the same trend when comparing their preferred tautomer between NMR and neutron crystallography, and it even seems consistent at the two pH values. His15 appears neutral in both neutron crystal structures with the ^{2}HNε2 being evident in the nuclear scattering length density maps (Figure S2) and is engaged with charged Lys118 as a hydrogen bond acceptor. The NMR also shows this tautomer to be the dominant form in solution, but partially protonated at pH 6. His36 is clearly charged at pH 6 and both occupancy and B-factors refine to similar values for ^{2}HNε2 and ^{2}HNδ1 (Table 3, Figure S2) and this is consistent with proton occupancies derived from the NMR data (Table 2). His 17 is a complex case in the NMR data, with a roughly equal distribution of the neutral tautomers (pH 10, Figure S3) and partially protonated at pH 6. The neutron crystallography data are consistent with this observation; however, one might incorrectly conclude that His 17 is protonated at pH 6.

In contrast, it is not clear for His10 as the density for the side chain suffers from signal cancellation and occupancies refine to zero despite the presence of some visible density (Figure S2 and S3). At pH 10, we see the opposite of what is measured using NMR: His10 is neutral with ^{2}HNδ1 as the only tautomer in the crystal structure. It is possible that HCA II molecules with this His10 tautomer preferentially crystallizes at pH 10, while NMR reports on all the molecules in solution. A more likely explanation is that the crystallographic data at pH 10 suffers from low completeness and is derived from a partially H/D exchanged protein.

The View on Proton Occupancies in Histidine from Both Neutron Crystallography and NMR

Neutron crystallography and NMR spectroscopy are both well suited to observe proton occupancies for histidines located in the interior of proteins. They usually only exist in one distinct state, making the interpretation of neutron crystallography data significantly easier. In addition, neutron crystallography provides the structural context of histidines, it allows the observation of the hydrogen bond patterns around the histidine and even complete hydrogen bond networks of the protein and nearby water molecules. NMR spectroscopy, on the other hand, requires additional methods, like X-ray or neutron crystallography, cryo-EM, or an NMR structure to provide the structural context. However, it can complement neutron crystallography in certain cases of ambiguity or imperfect data, in a rather fast and simple way. It is well-suited for at least medium sized proteins, and the histidine of interest can be assigned by mutation. For histidines located on or close to the protein surface the picture changes. Such histidines are often somewhat dynamic and co-exist in two or three different states and this has a negative impact on the interpretation of neutron crystal structures. Neutron crystallography often only allows the identification of the predominant state of the histidines, and might fail completely if the data is low resolution, incomplete, and/or the protein is only partially labeled. In contrast, NMR spectroscopy can provide the distribution of the three states and the overall proton occupancy with fairly high accuracy. Especially the distinction between the charged protonated state (His^+) and the two neutral deprotonated states (HNε2 and HNδ1) is very precise, since it is derived from accurate pK_a values, while the exact relative distribution of HNε2 and HNδ1 can be more challenging. It should be noted, that many of these "outside" histidines are functionally less important, so an NMR investigation might not be needed. Nevertheless, there are examples, in which "outside" histidines are important for Coulomb interactions, hydrogen bond relay switches, proton transfer, and catalysis. Things can get severely complicated, e.g., as is the case for His64 in HCA II, which shuttles protons in and out of the active site. It exists in two structural conformations, "in" and "out", at a roughly 50/50 distribution. In both states, it exists in two rotamers (orientation around chi-2), again at roughly 50/50 distribution. With pK_a values of 6.25 (inward) and 7.60 (outward), it is significantly protonated and positively charged, as well as deprotonated and neutral in the ensemble at the same time. Moreover, in its neutral state it exists in both tautomeric forms (HNε2 and HNδ1), at roughly a 50/50 distribution. On top of this all of these mentioned substates interconvert rapidly, which is a requirement for its function. In crystallography, some rotamers or tautomers can be preferentially "trapped" by manipulating the crystallization conditions. For example His64 can be seen to be charged and fully in the "out" conformation by acidifying the crystals to pH 6.[43] Complicated cases such as His64 fully warrant taking a combined, complementary approach using several methods such as NMR spectroscopy, neutron and X-ray crystallography, and computational methods.

Conclusions

The investigation into the protonation states and tautomer distribution of histidine residues within Human Carbonic Anhydrase II (HCA II) sheds light on the dynamic interplay between structure and pH dependence: buried residues remain predominantly neutral and adopt a single, preferred tautomer, while solvent-exposed residues display high variability in terms of proton occupancy but also in which particular tautomers were preferred. In order to fully capture the variance of histidines, the combination of neutron crystallography and NMR spectroscopy, both with their strengths and limitations, is crucial. While neutron crystallography can provide high-resolution structural information, it suffers from low completeness and difficult-to-interpret map, especially if proteins are only partially deuterated and if histidines co-exist in multiple states. In contrast, NMR spectroscopy can probe individual protons and offers insights into dynamic proton exchange in solution. Overall, the results from the two methods were broadly consistent. However, certain discrepancies between the two methods underscore the complexity of histidine behaviour and highlights the need for complementary approaches to fully elucidate enzyme mechanisms. This study advances our understanding of histidine protonation dynamics in HCA II and provides a foundation for future investigations into the role of histidines in enzyme catalysis.

Experimental Section

NMR Spectroscopy

Recombinant HCA II wild type and mutants were expressed in ModC1 minimal media with ^{13}C-glucose and/or $^{15}NH_4Cl$ to produce uniform ^{13}C- and/or ^{15}N labeled protein and purified as described previously.[14] For NMR measurements, 0.5 to 1.0 mM HCA II was dialyzed against 50 mM MES, MOPS, HEPES, TRIS/HCl or CAPS buffer and the pH was adjusted with NaOH or HCl on each sample (including 10% D_2O) and checked right before the measurement in the NMR tube at room temperature with an inoLab pH 720 pH meter equipped with a Hamilton Spintrode pH electrode. Aromatic ^{1}H-^{13}C ct HSQC spectra were performed on a Bruker Avance III spectrometer at a static magnetic field of 18.8 T at 308 K and multiple pH values. Assignments of histidines were reported previously.[14] The observed chemical shift δ_{obs} of the ^{1}Hδ2, ^{13}Cδ2, ^{1}Hε1, ^{13}Cε1 position were fitted in a global way[10] to the Henderson-Hasselbalch equation

$$\delta_{obs} = \frac{\delta_{HA} + \delta_{A^-} 10^{nH(pH-pK_a)}}{1 + 10^{nH(pH-pK_a)}}$$

with Hill parameter n_H. Errors were estimated by Monte-Carlo simulations with 1000 steps and a random variation of pH (±0.1) and ^{1}H (±0.01 ppm) and ^{13}C (±0.02 ppm) chemical shifts. The ratio of the two neutral (HNε2 and HNδ1) tautomeric forms was determined with

$$\Delta\delta = \frac{p_{HN\varepsilon 2}}{p_{HN\varepsilon 2} + p_{HN\delta 1}} \times \Delta\delta_{HN\varepsilon 2} + \frac{p_{HN\delta 1}}{p_{HN\varepsilon 2} + p_{HN\delta 1}} \times \Delta\delta_{HN\delta 1}$$

by the ^{15}Nε2, ^{15}Nδ1 and ^{13}Cδ2 chemical shifts in comparison to reference chemical shifts,[29] or by ^{2}J ^{1}H–^{15}N HSQC spectra of histidines.[30] Δδ is the observed chemical shift difference between protonated and deprotonated state and $\Delta\delta_{HN\varepsilon2}$ and $\Delta\delta_{HN\delta1}$ the chemical shift difference between protonated state and the corresponding tautomer. $p_{HN\varepsilon2}$ and $p_{HN\delta1}$ denotes the respective population. For error estimation, $\Delta\delta_{HN\varepsilon2}$ and $\Delta\delta_{HN\delta1}$ were varied about 17% of their difference. An example for the determination of HNε2 and HNδ1 from chemical shifts is shown in Figure 5.

Crystallography

The joint X-ray and neutron crystal structures used in this work came from PDB ID 3kkx (pH 10) and 4y0j (pH 6) from a previous study.[43,45] Since the structures were refined using different and obsolete software, and how models are prepared for refinement has changed, the models had to be modified to be suitable for joint X-ray/neutron refinement as it is done in PHENIX v.1.18.2-3874.[46] To enable this current study, the PDB models had to be manually manipulated in order to determine the charged state and relative occupancy of ^{2}H on the imidazole ring. Specifically, the His residues were initially modeled as charged with both ^{2}H present at full occupancy on the imidazole ring. Since ReadySet in PHENIX places both ^{1}H and ^{2}H atoms at the same position with 50/50 occupancy, the ^{1}H atoms had to be manually deleted, leaving only ^{2}H behind. Prior to refinement, occupancies were set at 1.0 and B-factors at 20.0 for the ^{2}H atoms on histidine Nε2 and Nδ1 positions (the rest of the model PDB was left "as is"). This was done for histidine residues: 3, 4, 10, 15, 17, 36, 107, and 122. His64, 94, 96, 119 were not included in this analysis due to their unique environments as described earlier. This was followed by model refinement of only the B-factor and occupancy parameters in PHENIX. This was followed by iterative rounds of manual inspection and modification of ^{2}H atoms on His side chains (only) in Coot followed by refinement in PHENIX[46]. Finally, ^{2}H atoms were deleted when there was no $2F_o$-F_c density for it in nuclear scattering length density maps or if negative F_o-F_c density appeared. In addition, any H-bonds to neighboring residues were taken into consideration (e.g., a clear and strong H-bond between Tyr194 and His107 with supporting $2F_o$-F_c density). This produced a model where relevant His residues had only ^{2}H in exchangeable positions remaining on Nε2 and/or Nδ1and only if they had visible density above sigma 1.0.

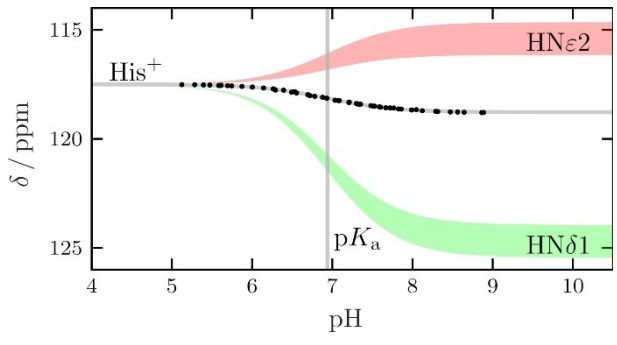

Figure 5. pH titration curve of His36 ^{13}Cδ2. Measured chemical shifts (black points, with error bars smaller than marker size) were fitted to the Henderson-Hasselbalch equation (gray curve). The pK_a value, at which the protonation ratio is balanced, is shown as a gray vertical line. In the basic pH range, the observed chemical shift reflects the population weighted averaged values of the two neutral (HNε2 and HNδ1) tautomeric forms. If the histidine was completely present in the HNε2 form, a titration curve in the red range would be expected, whereas if it was completely in HNδ1 form, it would fall in the green range.

Acknowledgements

This research was supported by the Deutsche Forschungsgemeinschaft (WE 5587/1-1 & WE 5587/1-2). Open Access funding enabled and organized by Projekt DEAL.

Conflict of Interests

The authors declare no conflict of interest.

Data Availability Statement

The data that support the findings of this study are available from the corresponding author upon reasonable request.

Keywords: Carbonic anhydrase · Enzymes · Histidine · Neutron protein crystallography · NMR spectroscopy · Protonation

[1] G. A. Jeffrey, W. Saenger, Springer, Berlin,, **1991**resource.
[2] T. E. Creighton Helvetian Press, **2010**.
[3] A. Warshel, J. Aqvist, *Ann. Rev. Biophys. Biophys. Chem.* **1991**, *20*, 267–298.
[4] A. Warshel, P. K. Sharma, M. Kato, Y. Xiang, H. B. Liu, M. H. M. Olsson, *Chem. Rev.* **2006**, *106*, 3210–3235.
[5] M. Eigen, *Angew. Chem. Int. Edit.* **1964**, *3*, 1-&.
[6] A. Fersht, *Enzyme Structure and Mechanism*, W. H. Freeman, **1977**.
[7] G. J. Bartlett, C. T. Porter, N. Borkakoti, J. M. Thornton, *J. Mol. Biol.* **2002**, *324*, 105–121.
[8] G. L. Holliday, J. B. O. Mitchell, J. M. Thornton, *J. Mol. Biol.* **2009**, *390*, 560–577.
[9] W. F. Reynolds, I. R. Peat, M. H. Freedman, J. R. Lyerla Jr., *J. Am. Chem. Soc.* **1973**, *95*, 328–331.
[10] H. N. Raum, U. Weininger, *ChemBioChem* **2019**, *20*, 922–930.
[11] H. N. Raum, K. Modig, M. Akke, U. Weininger, *J Am Chem Soc* **2024**, *146*, 22284–22294.
[12] M. R. Jensen, M. A. Hass, D. F. Hansen, J. J. Led, *Cell. Mol. Life Sci.* **2007**, *64*, 1085–1104.
[13] S. Lindskog, *Pharmacol. Ther.* **1997**, *74*, 1–20.
[14] H. N. Raum, S. Z. Fisher, U. Weininger, *Cell Mol. Life Sci.* **2023**, *80*, 286.
[15] M. R. Preimesberger, A. Majumdar, S. L. Rice, L. Que, J. T. Lecomte, *Biochemistry* **2015**, *54*, 6896–6908.
[16] R. N. Krishna Deepak, R. Sankararamakrishnan, *Biochemistry* **2016**, *55*, 3774–3783.
[17] S. Styring, J. Sjoholm, F. Mamedov, *Biochim. Biophys. Acta.* **2012**, *1817*, 76–87.
[18] C. V. Pagba, T. G. McCaslin, S. H. Chi, J. W. Perry, B. A. Barry, *J Phys. Chem. B* **2016**, *120*, 1259–1272.
[19] J. Wang, N. Tochio, R. Kawasaki, Y. Tamari, N. Xu, J. Uewaki, N. Utsunomiya-Tate, S. Tate, *Biochemistry* **2015**, *54*, 5242–5253.
[20] J. Hu, R. Fu, K. Nishimura, L. Zhang, H. X. Zhou, D. D. Busath, V. Vijayvergiya, T. A. Cross, *Proc. Natl. Acad. Sci. U S A* **2006**, *103*, 6865–6870.
[21] A. Cohen, Y. Ben-Abu, S. Hen, N. Zilberberg, *J Biol Chem* **2008**, *283*, 19448–19455.
[22] E. Oksanen, J. C. H. Chen, S. Z. Fisher, *Molecules* **2017**, *22(4),* 596-621.
[23] W. B. O'Dell, A. M. Bodenheimer, F. Meilleur, *Arch. Biochem. Biophys.* **2016**, *602*, 48–60.
[24] F. Kono, K. Kurihara, T. Tamada, *Biophys. Physicobiol.* **2022**, *19,* e190009..
[25] A. P. Duff, in *Proceedings of the 3rd International Symposium of Quantum Beam Science at Ibaraki University "Quantum Beam Science in Biology and Soft Materials (ISQBSS2018)", Vol. 25*, Journal of the Physical Society of Japan, **2019**.
[26] P. D. Adams, M. Mustyakimov, P. V. Afonine, P. Langan, *Acta Crystallogr. D Struct. Biol.* **2009**, *65*, 567–573.
[27] M. A. S. Hass, F. A. A. Mulder, *Ann. Rev. Biophys.* **2015**, *44*, 53–75.

[28] S. Lindman, S. Linse, F. A. A. Mulder, I. Andre, *Biophys. J.* **2007**, *92*, 257–266.
[29] G. Platzer, M. Okon, L. P. McIntosh, *J. Biomol. NMR* **2014**, *60*, 109–129.
[30] J. G. Pelton, D. A. Torchia, N. D. Meadow, S. Roseman, *Prot. Sci.* **1993**, *2*, 543–558.
[31] J. A. Vila, Y. A. Arnautova, Y. Vorobjev, H. A. Scheraga, *Proc. Natl. Acad. Sci. USA* **2011**, *108*, 5602–5607.
[32] J. Wallerstein, U. Weininger, M. A. Khan, S. Linse, M. Akke, *J. Am. Chem. Soc.* **2015**, *137*, 3093–3101.
[33] D. N. Silverman, S. Lindskog, *Acc. Chem. Res.* **1988**, *21*, 30–36.
[34] D. N. Silverman, R. Mckenna, *Acc. Chem. Res.* **2007**, *40*, 669–675.
[35] C. K. Tu, D. N. Silverman, C. Forsman, B. H. Jonsson, S. Lindskog, *Biochemistry* **1989**, *28*, 7913–7918.
[36] Z. Fisher, J. A. H. Prada, C. Tu, D. Duda, C. Yoshioka, H. Q. An, L. Govindasamy, D. N. Silverman, R. McKenna, *Biochemistry* **2005**, *44*, 1097–1105.
[37] T. K. Paul, S. Taraphder, *J. Phys. Chem. B* **2022**, *126*, 1413–1425.
[38] S. Z. Fisher, C. M. Maupin, M. Budayova-Spano, L. Govindasamy, C. Tu, M. Agbandje-McKenna, D. N. Silverman, G. A. Voth, R. McKenna, *Biochemistry* **2007**, *46*, 2930–2937.
[39] S. K. Nair, D. W. Christianson, *J. Am. Chem. Soc.* **1991**, *113*, 9455–9458.
[40] D. Rai, S. Khatua, S. Taraphder, *ACS Omega* **2022**, *7*, 31149–31166.
[41] D. Rai, D. Mondal, S. Taraphder, *J. Phys. Chem. B* **2023**, *127*, 10279–10294.
[42] H. Shimahara, T. Yoshida, Y. Shibata, M. Shimizu, Y. Kyogoku, F. Sakiyama, T. Nakazawa, S. Tate, S. Ohki, T. Kato, H. Moriyama, K. Kishida, Y. Tano, T. Ohkubo, Y. Kobayashi, *J. Biol. Chem.* **2007**, *282*, 9646–9656.
[43] R. Michalczyk, C. J. Unkefer, J. P. Bacik, T. E. Schrader, A. Ostermann, A. Y. Kovalevsky, R. McKenna, S. Z. Fisher, *Proc. Natl. Acad. Sci. USA* **2015**, *112*, 5673–5678.
[44] D. Liebschner, P. V. Afonine, N. W. Moriarty, P. D. Adams, *Method Enzymol.* **2020**, *634*, 225–255.
[45] S. Z. Fisher, A. Y. Kovalevsky, J. F. Domsic, M. Mustyakimov, R. McKenna, D. N. Silverman, P. A. Langan, *Biochemistry* **2010**, *49*, 415–421.
[46] D. Liebschner, P. V. Afonine, B. K. Poon, N. W. Moriarty, P. D. Adams, *Acta. Crystallogr. D Struct. Biol.* **2023**, *79*, 1079–1093.

Manuscript received: November 13, 2024
Revised manuscript received: December 16, 2024
Accepted manuscript online: December 17, 2024
Version of record online: January 2, 2025